Heliyon 10 (2024) e38896

Contents lists available at ScienceDirect

Heliyon

journal homepage: www.cell.com/heliyon

Research article

The fracture and perforation failure analysis of downhole tubes

H. Ding [a,b,*], H.B. Li [a,**], Z. Zhang [a], D.T. Qi [a], G.Q. Qi [a,b], X.H. Cai [a]

[a] *Tubular Goods Research Institute, China National Petroleum Corporation & State Key Laboratory of Oil and Gas Equipment, Shaanxi, Xi'an, 710065, China*

[b] *Department of Applied Chemistry, School of Science, Northwestern Polytechnical University, Xi'an, 710072, China*

ARTICLE INFO

Keywords:
Downhole tube
Fracture
Perforation
Corrosion
SSCC
pH value

ABSTRACT

: The downhole tubes were fractured and perforated after 5 years of shut-in due to high water cuts. This study employs a comprehensive array of analytical techniques to investigate the mechanisms behind fractures and perforations. Utilizing non-destructive testing (NDT), direct reading spectrometer, tensile strength testing machine, impact testing machine, optical microscope (OM), macroscopic fracture morphology observation, scanning electron microscope (SEM) and energy spectrum analysis (EDS), and sulfide stress corrosion cracking (SSCC) was studied. The reason for the fracture of the tubing is that under the condition of low pH value, high hydrogen sulfide environment, the tubing is fractured due to stress concentration caused by cracks in the outer thread relief groove. The perforation of the inner tube wall was caused by gradual wall thickness reduction under the influence of H_2S, CO_2, and Cl^-, resulting in fouling and eventual perforation. To prevent tube corrosion during long-term shut-in, it is recommended to inject crude oil or diesel into the well.

1. Introduction

The deep oil and gas reservoirs in the oil fields in western China are extremely difficult to exploit. The harsh environment of high temperature, high pressure, high salinity, and high hydrogen sulfide and carbon dioxide is a rare problem in the world [1,2]. As a downhole fluid production channel, the tubing needs to overcome the harsh working conditions of the deep underground environment [3,4]. The tube body and thread should bear a high axial load, and the material needs to bear the corrosion of the medium to serve safely.

In Liu's research [5], the stress corrosion cracking (SCC) properties of X70 pipeline steel were meticulously examined in an acidic soil extract through the employment of a slow strain rate test (SSRT). The findings revealed a stark contrast in SCC susceptibilities between two different microstructural conditions: the quenched steel, characterized by a bainitic structure, demonstrated a heightened vulnerability to SCC when exposed to the acidic soil environment. Meresht studied stress corrosion cracking occurring in a gas transmission steel pipeline, the chemical interactions and formation of carbonate/bicarbonate solution and with the presence of tensile stresses, stress corrosion cracking occurred in the longitudinal-direction and at the outer surface of the pipe [6]. Shi investigated stress corrosion cracking (SCC) in carbon steel pipes, the nucleation and propagation of cracks due to a combined effect of mechanical stress and chemical corrosion, which may lead to unexpected failure [7]. Li's investigation delved into the impact of microstructural

* Corresponding author. Tubular Goods Research Institute, China National Petroleum Corporation & State Key Laboratory of Oil and Gas Equipment, Shaanxi, Xi'an, 710065, China.

** Corresponding author.

E-mail addresses: dinghan@cnpc.com.cn (H. Ding), lihoubu@cnpc.com.cn (H.B. Li).

https://doi.org/10.1016/j.heliyon.2024.e38896
Received 27 June 2023; Received in revised form 28 September 2024; Accepted 1 October 2024
Available online 2 October 2024

elements within the heat-affected regions of high-strength pipeline steels on their propensity for stress corrosion cracking in an acidic soil setting. The findings highlighted that among the microstructural features, the specific arrangement of the M-A (martensite-austenite) phase was notably influential on the steel's sensitivity to SCC, as evidenced by Ref. [8]. Researchers Wu [9], Liao [10], and Ke [11] examined instances of leakage in shale gas gathering pipelines, attributing the failures to the corrosive effects of sulphate-reducing bacteria (SRB), carbon dioxide, oxygen, and chloride ions. Liu Yucheng [12] researched corrosion perforation on the pipeline by a medium of high salinity acidic oil-water mixture. The result showed that non-uniform corrosion occurred on the surface of the coupon, and the corrosion rate of weight loss was 0.187 mm/y The corrosion products were mainly ferrous sulfide (FeS) and silicon disulfide (SiS_2), and the scaling was mainly calcium carbonate ($CaCO_3$). Zhiyong Liu [13] investigated a perforation L415 steel gas pipeline. The results revealed that the material composition and organization of the steel pipe conformed to API Specification 5CT. Ni [14] studied an abnormal perforation of a super-large diameter-buried gas pipeline near the metro. The findings revealed that impurities accumulated from water gas led to localized corrosion on the underside of the pipeline's inner wall, resulting in the development of corrosion pits. Li [15] investigated the perforation of the L360M pipeline in the liquefied natural gas transmission process. The pipeline perforation is understood to progress through three successive stages: (a) the onset of corrosion scale formation and pitting, (b) the amplification of scale thickness and pitting advancement, and (c) the accumulation of scales and further pit expansion. Notably, during the LNG transmission, the accumulated scales serve to expedite the enlargement of these corrosion pits.

While numerous researchers [16–19] have extensively examined the fractures and corrosion-induced perforations in pipes and equipment employed in oil and gas fields, there exists a scarcity of literature addressing the combined phenomena of both fracture and perforation specifically in downhole tubing. The downhole conditions are complex, and the service environment of the tube is extremely harsh. In this paper, we analyze the causes of fracture and perforation of downhole tubes to avoid the recurrence of similar incidences.

During the killing operation of a well in the western oil field, it was found that the 66th (approximately 630m) and 73rd (approximately 690m) tubes were fractured and failed. The fracture positions were all located at the root of the connecting thread of the tube. The 243rd (approximately 2310m) tube body was corroded and perforated. The specifications of the failed tubes were Φ88.9 mm × 6.45 mm, and the steel grade was BG110S. They were marked as 1#, 2#, and 3#, respectively. The macroscopic morphology is shown in Fig. 1.

The well was drilled in June 2010 and completed in October 2010. It is an evaluation well with a depth of 5463.44 m. In November 2012, the 8 mm choke was shut down for producing a high water cut. The lack of formation energy in this well led to wellbore effusion and the rapid rise of water cuts. In August 2017, the well-killing operation began, and the return fluid was abnormal, and the well was blocked. During the salvage operation, the 66th tubing was broken, the 73rd tubing was broken, and the 243rd tubing was corroded and perforated.

According to the information provided by the client, the fluid properties of the well are shown in Table 1. The produced water in this well is a typical calcium chloride water type, and the chloride ion content is as high as 116000 mg/L; the hydrogen sulfide content in the produced gas of the well is as high as 205000 mg/m^3, and the carbon dioxide content is 3.65 %. Judging from the working environment parameters, the fluid medium of the well has strong corrosion to carbon steel materials.

2. Experimental

In order to uncover the underlying causes of fracture and perforation failures in downhole tubing, an exhaustive experimental study was conducted, involving comprehensive analysis of the sample's failure mechanisms. Fluorescent magnetic particle inspection, a form of nondestructive testing (NDT), was employed to locate cracks in the vicinity of the fracture site. Chemical composition analysis of both the base metal of the downhole tube and the fractured section was performed using an ARL4460 optical emission spectrometer. Furthermore, the tensile strength and yield strength of the base metal at ambient temperature were assessed using a UTM-5305 universal testing machine. To evaluate the material's resistance to sudden impacts at low temperatures, the PIT752D-2(300J) impact tester was utilized to determine the base metal's impact energy at −10 °C. These tests collectively provided a thorough understanding of the downhole tubing's fracture and perforation mechanisms. Additionally, the microstructure of the fracture zone was meticulously examined using the OLS-4100 laser confocal microscope. To gain deeper insights, the fracture and perforation surfaces were scrutinized under an optical microscope (OM), a scanning electron microscope (SEM), and underwent energy dispersive

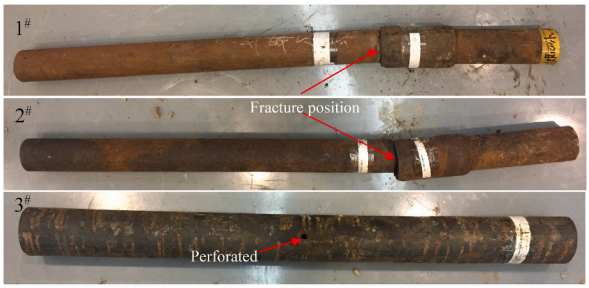

Fig. 1. The visual appearance of the failed tubes.

Table 1
Well flow properties.

Water parameters					
Horizon	Density(g/cm^3)	Cl^-(mg/L)	Mineralization (mg/L)		Water classifying
O	5.12	116000	0.769		Calcium chloride
Oil parameters					
Horizon	20 °C Density(g/cm^3)	Asphaltene (wt%)	Colloid (wt%)	Sulfur (wt%)	Wax (wt%)
O	0.8110	1.84	1.75	0.409	7.2
Gas parameters					
Horizon	Density(kg/m^3)	CO_2 (vol%)	H_2S (mg/m^3)		CH_4 (vol%)
O	0.7797	3.65	205000		68.9

spectroscopy (EDS) analysis for elemental composition. As a final step in the investigative process, a laboratory simulation of sulfide stress corrosion cracking (SSCC) was performed on a replicate of the failed sample to replicate and study the corrosion conditions that potentially led to the failure. This comprehensive approach integrated visual, compositional, and simulated corrosion testing to thoroughly discern the fracture and perforation mechanisms.

3. Results and analysis

3.1. Nondestructive testing

According to ASTM E709-2015 [20], the results of fluorescent magnetic particle testing (FMPT) near the fracture position are shown in Fig. 2. The test results indicate that aside from the primary fracture, no additional cracks or defects were detected on the outer surface of the affected tube segment.

3.2. Chemical composition

The spectral analysis of the material composition in the vicinity of the fracture section and the base metal of Tube 1#, as depicted in Fig. 1, yielded results summarized in Table 2. These findings confirm that the chemical composition of both the area close to the fracture and the base metal conform to the specifications outlined in TLM-JSXY-YG-2015-1 [21], thereby meeting the required standards.

3.3. Mechanic property analysis

In adherence to the guidelines of ASTM A370-17 [22], the tensile testing results for the base metal of Tube 1# at room temperature are tabulated in Table 3. These outcomes illustrate that the tensile strength, yield strength, and elongation performance parameters all satisfy the criteria specified in TLM-JSXY-YG-2015-1 [21], indicating compliance with the standard.

Following the procedures outlined in ASTM E23-16b [23], the results of the impact energy tests conducted on the specimen at room temperature are summarized in Table 4. The test outcomes demonstrate that the impact resistance of the steel pipe fulfills the criteria set forth in TLM-JSXY-YG-2015-1 [21], thereby confirming its satisfactory impact performance.

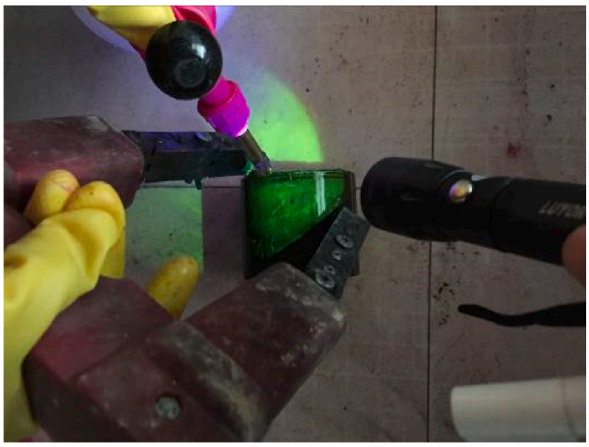

Fig. 2. Magnetic particle testing around the outer surface of the fracture tube section.

Table 2
Chemical composition of steel pipe (wt.%).

Element	C	Si	Mn	P	S	Cr	Mo	Ni	Ti
Base metal	0.29	0.24	0.43	0.0055	0.001	0.49	0.80	0.035	0.0024
Fracture section	0.28	0.23	0.44	0.0055	0.0013	0.53	0.80	0.031	0.0024
TLM-JSXY -YG-2015-1	/	/	/	≤0.015	≤0.005	/	/	/	/

Table 3
Tensile test results at room temperature.

Sample No.	Width × Gauge length (mm)	Tensile Strength (MPa)	Yield Strength (MPa)	Elongation (%)
1#	19.1 × 50	842	790	22
2#		834	778	22
3#		854	795	23
TLM-JSXY-YG-2015-1		≥793	758~828	≥16

3.4. Metallographic analysis

A sample was extracted and prepared from the fractured region of Tube 1 for further examination. The structure, grain size, and nonmetallic inclusion of the sample were analyzed. The analysis results show that the nonmetallic inclusions around the fracture are A0.5, B0.5, and D0.5. Visible cracks are evident on the outer surface of the fracture area. (Fig. 3ã3c), there are local intergranular cracks along the crack direction, and the cracks propagate downward along the fracture to the 2/3 position of the wall thickness. The microstructure around the fracture and crack is tempered martensite and some ferrite, and there is no abnormality in the microstructure (Fig. 3d). The grain size is 11.0.

3.5. Macroscopic morphology analysis

The overall appearance of the fracture on Tube 1# is illustrated in Fig. 4a, providing a macroscopic view of the damage. The fracture has completely traversed the material in the transverse direction, with its position specifically pinpointed at the segment housing the thread's common buckle recess groove. It is completely broken along the transverse direction, and the fracture position is located at the part of the thread common buckle retreating groove. Thread processing is first end-face processing, then boring inner hole steps and cones, followed by thread processing. The quality of thread processing is affected by processing technology, clamping methods, processing equipment, tools, and cooling methods. The fracture surface is dark brown, and there is no obvious necking deformation around the fracture. The section is divided into two characteristic areas: flat area and shear lip area. The flat area accounts for about 1/4 of the circumference of the fracture and has brittle cracking characteristics. The shear lip area accounts for about 3/4 of the circumference of the fracture, which is the instantaneous fracture area formed by the final fracture of the tube. The macromorphology of the fracture of the 2# tube is shown in Fig. 4b. Due to the fishing operation, the fracture is smoothed, and the original fracture morphology is not observed. However, the cracking site is the same as the fracture site of the 1# tube, and it is also located at the part of the thread common buckle back groove. The inner surface of the perforation part of the 3# tube is shown in Fig. 4c. There are several corrosion products on the surface, and there is a scaling phenomenon. Fig. 4d shows the cross-section of the tubing at the perforation site. Observations reveal a substantial accumulation of debris within the tube, which has led to a notable thinning of the tube wall due to the buildup. The minimal thickness measured for the tube wall was merely 2.2 mm.

3.6. Electron microscope analysis

Samples were taken from the fracture site of 1# tube and the perforation site of 3# tube, respectively. The microscopic details of the fracture are depicted in Fig. 5a, where the fracture surface exhibits characteristics of brittle fracturing. Under magnification, there is no evidence of corrosion products covering the fracture surface. The morphology near the perforation site is shown in Fig. 5b, and the surface is covered by much loose white corrosion products.

The elemental composition of the fracture surface, crack, and perforation site were examined using Energy Dispersive Spectroscopy

Table 4
Impact test result (J).

Sample No.	Size (mm)	Notch	Temperature (°C)	Measured (J)	Equivalent value[a] (J)	TLM-JSXY-YG-2015-1
1#	5 × 10 × 55	V	−10	82	149	≥80J
2#				86	156	
3#				83	151	

[a] Note: The impact test value of 10 × 10 × 55 mm impact sample was converted according to API 5CT [24].

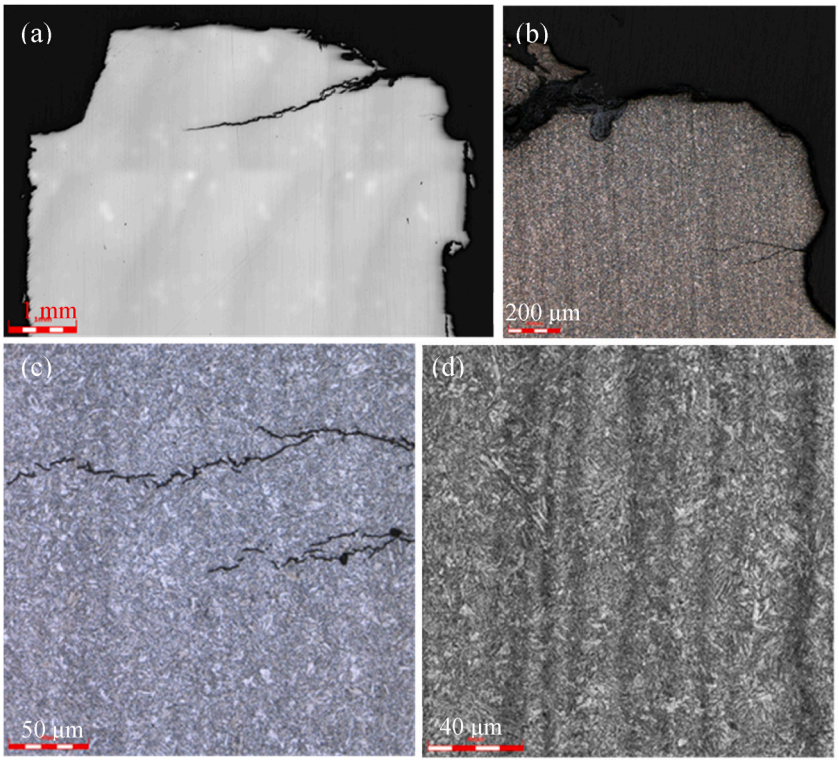

Fig. 3. Fracture crack and metallographic structure analysis (a) Fracture appearance; (b) Crack morphology of the fracture surface; (c) Crack surface profile; (d) Metallurgical structure of the fracture.

(EDS), with the findings illustrated in Figs. 6–8, respectively. Analysis revealed that the fracture surface is predominantly comprised of C, O, S, Ca, and Fe. The crack, on the other hand, contains primarily C, O, Fe, alongside trace amounts of S, Cl, and Ca. Furthermore, the corrosion products at the perforation site are mainly constituted by C, O, S, Cl, Ca, and Fe.

3.7. Sulfide stress corrosion cracking analysis

According to the NACE Standard TM 0177–2016 [25], the SSCC test was carried out on the samples near the fracture of 1# and 2# tube, respectively. The loading stress was 90 % of the measured minimum yield strength. After soaking in H_2S saturated solution (A solution) for 720 h, the test results are shown in Table 5, and the macroscopic morphology of the sample surface after the test is shown in Figs. 9 and 10. The test results show that all samples are not broken after soaking for 720 h and no cracks were found when magnified 10 times.

4. Discussion

4.1. Material analysis

Based on the test results and analysis above, the chemical composition, room temperature tensile strength, yield strength, elongation, and impact properties of the sample from 1# tube meet the requirements of TLM-JSXY-YG-2015-1. There was also no abnormality in the metallographic structure.

4.2. Cause analysis of tube fracture

First of all, according to the fluid properties of the well, the well is high in Cl^-, H_2S, and CO_2, and its working environment is very corrosive to carbon steel. Second, from the macroscopic morphology of the fracture, the fracture source area of 1# and 2# tubes is located at the cutter groove on the outer surface of the connecting thread of the tube. The finite element analysis of the stress distribution of the thread joint shows that this part is the highest stress part of the whole thread joint and the largest stress distribution point of the whole tube. In addition, it can be seen from the metallographic analysis results of the fracture that there are visible cracks on the fracture and the outer surface of the thread, and the crack extends to the position of 2/3 wall thickness, which further proves that the fracture of the tube originates from the root of the thread outside the tube. Microscopic analysis of the fracture surface shows

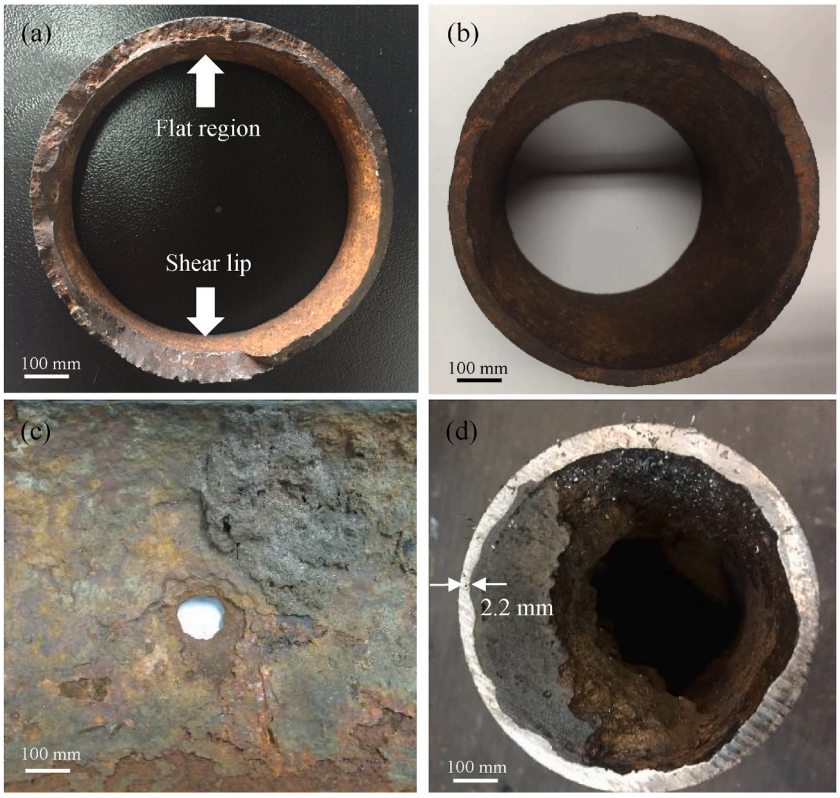

Fig. 4. Macroscopic morphology of fracture and perforation (a) Macroscopic fracture morphology of 1 # tube; (b) Macroscopic fracture morphology of 2 # tube; (c) Inner surface morphology of perforation site; (d) Internal scaling morphology of perforated tubing.

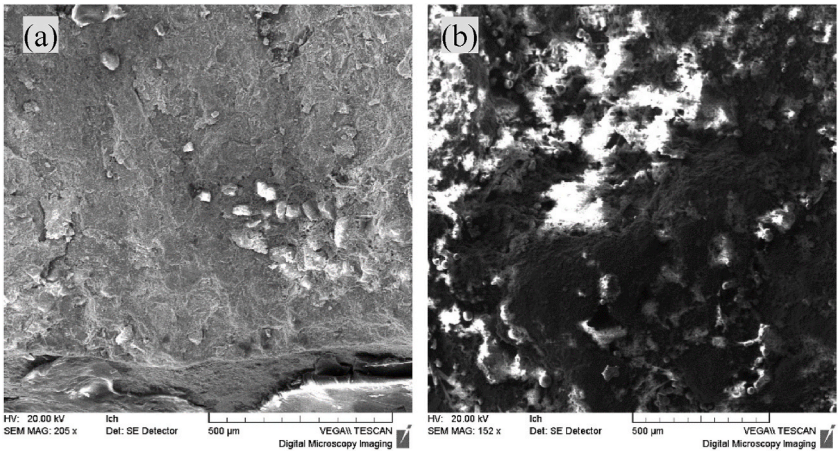

Fig. 5. SEM photo of the failure tube (a) The fracture source area of 1# tube; (b) The perforation site of 2# tube.

that its morphology is brittle cracking. The energy spectrum analysis of the fracture site reveals a surface composition primarily of Carbon (C), Oxygen (O), Sulfur (S), Calcium (Ca), and Iron (Fe) elements. Remarkably, this elemental profile mirrors that found within the crack on the outer fracture surface, with Sulfur (S) being a consistent constituent in both instances.

Taking into account the macroscopic appearance of the fractured tube, the microstructural characteristics of the cross-section, the metallographic examination of the crack, the energy spectrum analysis of the cross-section, and factoring in the investigation of the tube's operational conditions, it is conclusively determined that the tube's fracture is a classic case of sulfide stress corrosion cracking (SSCC).

The results of the sulfide stress corrosion cracking (SSCC) test show that the four-point bending specimen of 1# and 2 # tubes did not break after soaking in A-solution for 720 h, and no crack was found after 10 times magnification. Indicating that the SSCC

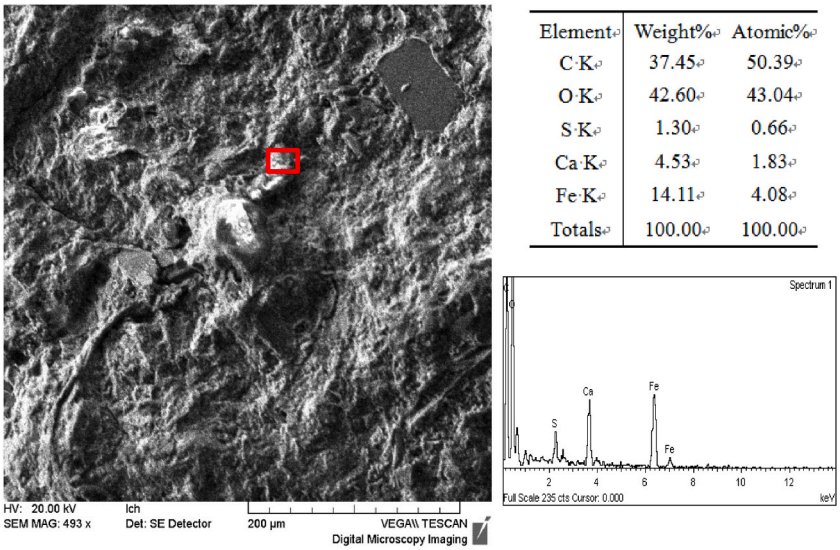

Element	Weight%	Atomic%
C K	37.45	50.39
O K	42.60	43.04
S K	1.30	0.66
Ca K	4.53	1.83
Fe K	14.11	4.08
Totals	100.00	100.00

Fig. 6. The EDS analysis of the fracture surface.

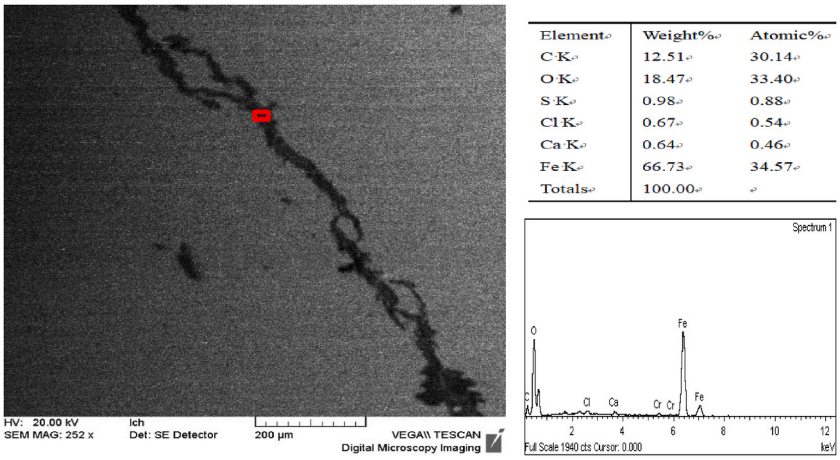

Element	Weight%	Atomic%
C K	12.51	30.14
O K	18.47	33.40
S K	0.98	0.88
Cl K	0.67	0.54
Ca K	0.64	0.46
Fe K	66.73	34.57
Totals	100.00	

Fig. 7. The EDS analysis of the crack.

resistance of the tube in a standard solution meets the requirements. However, from the tube service conditions, it can be seen that the well has a shut-in history of about 5 years. The content of hydrogen sulfide (H_2S) in the produced gas of the well is as high as 205000 mg/m^3, as shown in Table 1. Under the high pressure of bottom hole (5–15 MPa) with high temperature (123.5 °C) and well depth of 5425 m, H_2S might dissolve in the wellbore effusion, resulting in a decrease in pH value. As shown in Fig. 11, when the pH value in the solution is reduced, carbon steel and low alloy steel still have a greater risk of SSCC under smaller H_2S partial pressure [26]. In the case of high H_2S environment, crack defects (Fig. 3) in the thread relief groove led to failure, which caused by H_2S stress corrosion cracking with the increase of time.

Based on the above, the fracture of the tube belongs to SSCC, which is caused by the stress corrosion cracking of the original sulfur-resistant tubing in low pH medium after 5 years of shut-in of the well.

4.3. Cause analysis of tube perforation

There are a large number of corrosion products on the inner surface of the 3# tube perforation part, and there is a scaling phenomenon (Fig. 4c). The wall thickness around the inner surface corrosion pit is thinned, indicating that the part is perforated from inside to outside. From the cross-section of the tube at the perforation site, it can be observed that there is a large amount of fouling material inside the tubing, and the inner wall of the tubing is thinned (Fig. 4d). The thinnest part of the tube section is only 2.2 mm, which is 1/3 of the original wall thickness of the tube. Microscopic analysis shows that there are a large number of corrosion products at the perforation site (Fig. 5b). The corrosion products at the perforation site are mainly composed of C, O, S, Cl, Ca and Fe. Therefore,

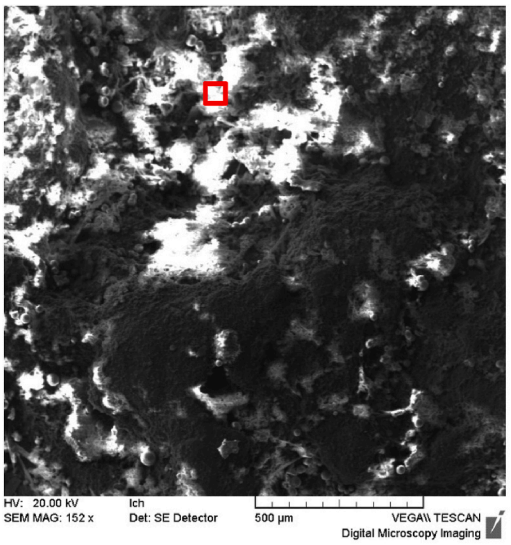

Element	Weight%	Atomic%
C K	68.58	81.34
O K	13.67	12.17
S K	6.10	2.71
Cl K	2.81	1.13
Ca K	3.91	1.39
Fe K	4.94	1.26
Totals	100.00	100.00

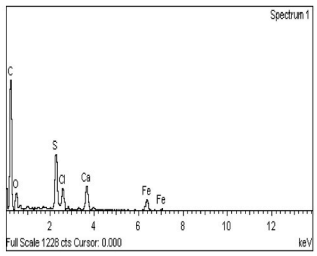

Fig. 8. EDS result of the perforation site.

Table 5
Sulfide stress cracking test conditions and test results.

Tube No.	Loading stress (MPa)	Sample No.	Test result
1#	788MPa × 90%	1–1 1–2 1–3	Not broken after soaking for 720 h and no cracks were found when magnified 10 times.
2#	788MPa × 90%	2–1 2–2 2–3	Not broken after soaking for 720 h and no cracks were found when magnified 10 times.

Fig. 9. Macroscopic photos of the 1# tube sample after 720 h of SSCC.

Fig. 10. Macroscopic photos of the 1# tube sample after 720 h of SSCC.

the inner wall of the tube is gradually thinned under the action of H_2S, CO_2, and Cl^-, forming fouling and eventually perforation.

5. Conclusions and preventive actions

1. The physical and chemical properties of the 1# tube sample meet the requirements of TLM-JSXY-YG-2015-1.
2. The reason for the fracture of the tubing is that under the condition of low pH value, high hydrogen sulfide environment, the tubing is fractured due to stress concentration caused by cracks in the outer thread relief groove.

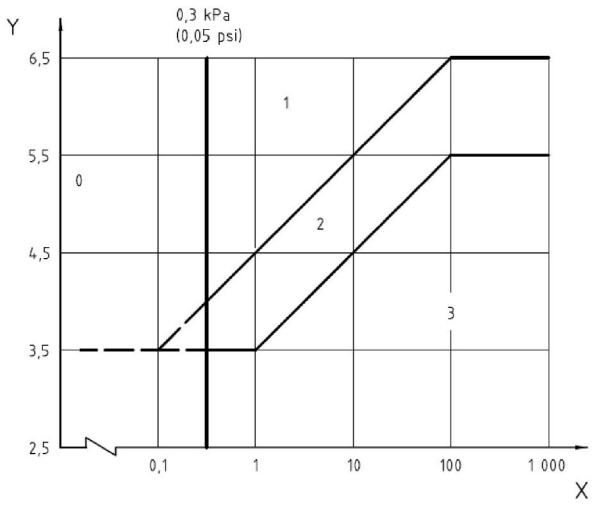

Fig. 11. SSC diagram of carbon steel and low alloy steel in different environments
(X axis is H_2S partial pressure (KPa), Y axis is the solution pH value).

3. The perforation of the tube's inner wall can be attributed to a gradual thinning of the wall over time, brought about by the corrosive effects of hydrogen sulfide (H_2S), carbon dioxide (CO_2), and chloride ions (Cl^-). This process leads to the accumulation of debris, or fouling, which ultimately culminates in the perforation of the wall.
4. It is recommended to prevent tube corrosion by injecting crude oil or diesel into the well during long-term shut-in.

Data availability statement

Data will be made available on request

Ethics declarations

Review and/or approval by an ethics committee was not needed for this study because the submission does not include human or animal participation.

CRediT authorship contribution statement

H. Ding: Software, Methodology, Investigation, Conceptualization. **H.B. Li:** Supervision, Funding acquisition, Conceptualization. **Z. Zhang:** Visualization, Investigation. **D.T. Qi:** Writing – review & editing, Data curation. **G.Q. Qi:** Visualization, Software, Methodology. **X.H. Cai:** Writing – review & editing, Visualization.

Declaration of competing interest

We declare that we have no financial and personal relationships with other people or organizations that can inappropriately influence our work, there is no professional or other personal interest of any nature or kind in any product, service and/or company that could be construed as influencing the position presented in, or the review of the manuscript entitled.

References

[1] A. Shadravan, M. Amani, What every engineer or geoscientist should know about high pressure high temperature wells, SPE Kuwait International Petroleum Conference and Exhibition (2012). Kuwait City, Kuwait, 2012.
[2] Nan Ji, et al., Collapse failure analysis of S13Cr-110 tubing in a high-pressure and high-temperature gas well, Eng. Fail. Anal. 148 (2023) 107187.
[3] Yunpeng Yang, et al., Multi-acoustic-wave-feature-based method for detection and quantification of downhole tubing leakage, J. Nat. Gas Sci. Eng. 102 (2022) 104582.
[4] Ting-ting Qu, et al., Investigation and analysis of fracture failure of TS-110 coiled tubing used in oil and gas field in southwest China, Eng. Fail. Anal. 147 (2023) 107153.
[5] Z.Y. Liu, et al., Stress corrosion cracking behavior of X70 pipe steel in an acidic soil environment, Corrosion Sci. 50 (2008) 2251–2257.
[6] E. Sadeghi Meresht, et al., Failure analysis of stress corrosion cracking occurred in a gas transmission steel pipeline, Eng. Fail. Anal. 18 (2011) 963–970.
[7] Chunxiang Shi, et al., Peridynamic investigation of stress corrosion cracking in carbon steel pipes, Eng. Fract. Mech. 219 (2019) 106604.
[8] Xueda Li, et al., Effect of microstructural aspects in the heat-affected zone of high strength pipeline steels on the stress corrosion cracking mechanism: Part I. In acidic soil environment, Corrosion Sci. 102 (2022) 104582.
[9] Guiyang Wu, et al., Analysis on corrosion-induced failure of shale gas gathering pipelines in the southern Sichuan Basin of China, Eng. Fail. Anal. 130 (2021) 105796.

[10] Ke Tong, et al., Analysis and investigation of the leakage failure on the shale gas gathering and transmission pipeline, Eng. Fail. Anal. 140 (2022) 106599.
[11] Kexi Liao, et al., Study on corrosion mechanism and the risk of the shale gas gathering pipelines, Eng. Fail. Anal. 128 (2021) 105622.
[12] Yucheng Liu, et al., Research on corrosion perforation on pipeline by media of high salinity acidic oil-water mixture, Eng. Fail. Anal. 34 (2013) 35–40.
[13] Zhiyong Liu, et al., Failure analysis of leakage caused by perforation in an L415 steel gas pipeline, Case Studies in Engineering Failure Analysis 9 (2017) 63–70.
[14] Ni Tong-Wei, et al., Failure analysis on abnormal perforation of super large diameter buried gas pipeline nearby metro, Eng. Fail. Anal. 103 (2019) 32–43.
[15] Xuanpeng Li, et al., Insights into the perforation of the L360M pipeline in the liquefied natural gas transmission process, Eng. Fail. Anal. 140 (2022) 106566.
[16] H. Ding, et al., Cracking analysis of a newly built gas transmission steel pipe, Eng. Fail. Anal. 118 (2020) 104868.
[17] A.Q. Fu, et al., Failure analysis of girth weld cracking of mechanically lined pipe used in gasfield gathering system, Eng. Fail. Anal. 68 (2016) 64–75.
[18] Mohsen Dadfarnia, et al., Assessment of resistance to fatigue crack growth of natural gas line pipe steels carrying gas mixed with hydrogen, Int. J. Hydrogen Energy 44 (2019) 10808–10822.
[19] Guoquan Qi, et al., Analysis of cracks in polyvinylidene fluoride lined reinforced thermoplastic pipe used in acidic gas fields, Eng. Fail. Anal. 99 (2019) 26–33.
[20] ASTM E709-2015 Standard Guide for Magnetic Particle Testing.
[21] TLM-JSXY-YG-2015-1 Tarim Oilfield Company Tubing Order Supplementary Technical Agreement.
[22] ASTM A370-17 Standard test methods and definitions for mechanical testing of steel products.
[23] ASTM E23-16b Standard test methods for notched bar impact testing of metallic materials.
[24] API 5CT Specification for casing and tubing.
[25] NACE Standard TM 0177-2016 Standard test method laboratory testing of metals for resistance to sulfide stress cracking and stress corrosion cracking in H2S environments.
[26] NACE MR0175/ISO 15156-2:2003(E) Petroleum and natural gas industries-Materials for use in H2S-containing environments in oil and gas production-Part 2: Cracking-resistant carbon and low alloy steels, and the use of cast irons.